2026, 51(5) DOI:10.11817/j.issn.1672-7347.2026.250446

·ARTICLES· ·论 著·

Targeting *ABCB6* induces ferroptosis in osteosarcoma cells via *HIF1A/GPX4* pathway

LIN Zili[1], LUO Hao[1], LI Xiangyao[1], LUO Wei[1, 2, 3]

[1. Department of Orthopaedics, Xiangya Hospital, Central South University, Changsha 410008; 2. National Clinical Research Center for Geriatric Disease (Xiangya Hospital of Central South University), Changsha 410008; 3. Bone and Joint Metabolism Medical Center, Xiangya Hospital, Central South University, Changsha 410008, China]

ABSTRACT

Objective: Osteosarcoma (OS) is a malignant bone tumor that predominantly affects adolescents. Due to its early metastatic tendency and chemoresistance, long-term survival rates in patients have not shown significant improvement over time, highlighting the urgent need for novel molecular targets and therapeutic strategies. Ferroptosis, a form of programmed cell death driven by iron-dependent lipid peroxidation, offers a promising avenue for overcoming drug-resistant tumors. ATP-binding cassette subfamily B member 6 (*ABCB6*) belongs to the ATP-binding cassette (ABC) transporter superfamily and is mainly localised to the outer mitochondrial membrane, where it participates in haem synthesis and intracellular iron transport. Recent studies have indicated that *ABCB6* is aberrantly expressed in various malignancies and regulates tumor progression, yet its role and mechanism in OS remain unexplored. The present study aims to systematically characterise the expression pattern, clinical prognostic significance, and biological functions of *ABCB6* in OS, and to dissect the molecular mechanism by which *ABCB6* governs ferroptosis in OS cells, thereby providing a theoretical foundation for *ABCB6*-targeted therapy.

Methods: Human OS cell lines (HOS and 143B) and human bone marrow mesenchymal stem cells (BMSCs) were used as research subjects. Stable *ABCB6*-knockdown OS cell lines were established via lentivirus-mediated RNA interference, and rescue experiments were performed using lentiviral overexpression of hypoxia-inducible factor 1-alpha (*HIF1A*). Cell proliferation was assessed by cell counting kit-8 (CCK-8) and colony formation assays; migration was evaluated by Transwell and scratch wound-healing assays; apoptosis was detected by flow cytometry. Ferroptosis-related phenotypic assays were employed to determine the impact of *ABCB6* expression on ferroptosis. Transcriptome sequencing was conducted to analyse differentially expressed genes and enriched

Date of reception: 2025-08-05
First author: LIN Zili, Email: woslinzili@163.com, ORCID: 0000-0003-3938-5705; LUO Hao, Email: drluohao@163.com, ORCID: 0009-0005-1605-7516
Corresponding author: LUO Wei, professor, Email: luoweixy@csu.edu.cn, ORCID: 0000-0003-1818-3469
Foundation item: This work was supported by the Health High-Level Talent Scientific Research Project of Hunan Province (R2023175), the Science and Technology Innovation Plan Project of Hunan Province (2023SK2023), China.
Open access: This is an open access article under Creative Commons Attribution-NonCommercial-NoDerivatives 4.0 International (CC BY-NC-ND 4.0) (https://creativecommons.org/licenses/by-nc-nd/4.0/).

©Journal of Central South University (Medical Science). All rights reserved.

pathways; chromatin immunoprecipitation (ChIP) and dual-luciferase reporter assays were applied to verify the direct binding of HIF1A to the promoter of glutathione peroxidase 4 (*GPX4*) and its transcriptional regulation. Iron chelator and proteasome inhibitor interventions were used to validate the regulation of HIF1A protein stability by Fe^{2+}. In vivo, *ABCB6*-knockdown and control 143B cells were injected subcutaneously into nude mice to establish a xenograft tumor model, and tumor growth was monitored.

Results: Both messenger RNA (mRNA) and protein levels of *ABCB6* were significantly higher in OS cell lines than in BMSCs (both $P<0.05$), and analysis of the Therapeutically Applicable Research to Generate Effective Treatments (TARGET)-OS cohort revealed that patients with high *ABCB6* expression had markedly worse overall survival than those with low expression [hazard ratio (*HR*)=2.94, 95% confidence interval (*CI*) 1.36 to 6.36, $P<0.05$]. *ABCB6* knockdown significantly suppressed OS cell proliferation and colony formation, reduced migratory capacity, and increased the apoptosis rate, accompanied by downregulation of N-cadherin and upregulation of E-cadherin and cleaved caspase-3 (all $P<0.05$). *ABCB6* silencing markedly elevated the proportion of Liperfluo-positive cells and dihydroethidium (DHE) oxidation levels, increased intracellular Fe^{2+} concentration, decreased the glutathione (GSH)/oxidized glutathione (GSSG) ratio, reduced mitochondrial membrane potential, and induced typical ferroptotic mitochondrial morphological changes (shrinkage and cristae reduction) as observed by transmission electron microscope (all $P<0.05$); these oxidative alterations were reversed by the ferroptosis inhibitors. *ABCB6* knockdown downregulated GPX4 at both protein and mRNA levels, whereas solute carrier family 7 member 11 (SLC7A11) expression remained unchanged ($P>0.05$). Transcriptome sequencing and Kyoto Encyclopedia of Genes and Genomes (KEGG) enrichment analysis showed significant enrichment of the HIF-1 signalling pathway in the control group ($P<0.001$); *ABCB6* knockdown decreased HIF1A protein expression, and treatment with an iron chelator or a proteasome inhibitor reversed this degradation through Fe^{2+} chelation or inhibition of the ubiquitin-proteasome pathway, respectively (all $P<0.05$). Chromatin immunoprecipitation followed by quantitative polymerase chain reaction (ChIP-qPCR) and dual-luciferase reporter assays confirmed that HIF1A directly binds to the *GPX4* promoter and activates its transcription. Overexpression of *HIF1A* in *ABCB6*-knockdown cells restored GPX4 expression and significantly rescued the proliferation inhibition, migration impairment, and apoptosis increase caused by *ABCB6* silencing, while also restoring mitochondrial membrane potential (all $P<0.05$). In the xenograft model, tumors from the *ABCB6*-knockdown group exhibited significantly reduced volume and weight compared with the control group (all $P<0.05$); immunohistochemistry confirmed downregulation of HIF1A and GPX4, reduced Ki-67 and N-cadherin positivity, and increased cleaved caspase-3 and E-cadherin positivity in the knockdown group (all $P<0.05$).

Conclusion: This study systematically uncovers, for the first time, the oncogenic role and prognostic value of *ABCB6* in OS, and delineates the complete "*ABCB6*/Fe^{2+}/*HIF1A*/*GPX4*" axis that governs ferroptosis in OS cells. These findings not only provide a novel biomarker for molecular subtyping and prognostic evaluation of OS, but also establish a theoretical basis for therapeutic strategies that target the *ABCB6*/*HIF1A*/*GPX4* axis to induce ferroptosis. Future investigations may explore the upstream regulators of *ABCB6* and its potential utility in reversing chemoresistance in OS.

©Journal of Central South University (Medical Science). All rights reserved.

Graphical Abstract

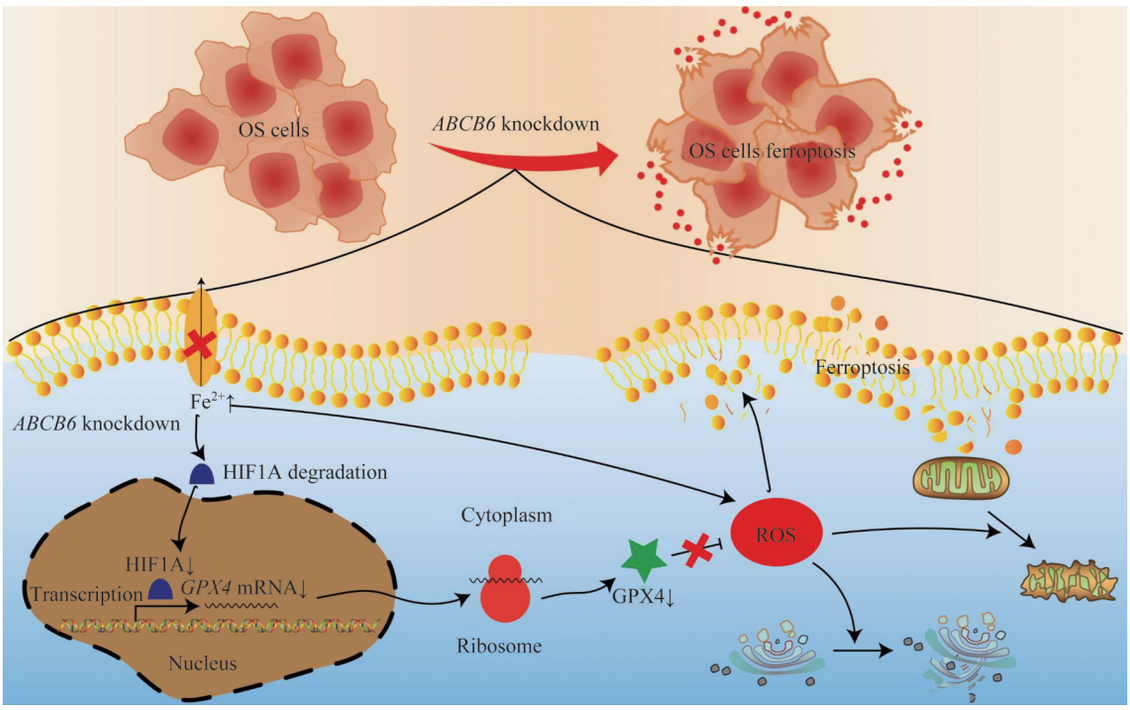

Targeting *ABCB6* induces ferroptosis in OS cells. *ABCB6*: ATP-binding cassette subfamily B member 6; OS: Osteosarcoma; HIF1A: Hypoxia-inducible factor 1-alpha; GPX4: Glutathione peroxidase 4; ROS: Reactive oxygen species.

KEY WORDS osteosarcoma; *ABCB6*; ferroptosis; *HIF1A*; *GPX4*

靶向*ABCB6*通过*HIF1A/GPX4*通路诱导骨肉瘤细胞铁死亡

林梓立[1]，罗浩[1]，李湘尧[1]，罗伟[1,2,3]

[1. 中南大学湘雅医院骨科，长沙 410008；2. 老年疾病国家临床医学研究中心(中南大学湘雅医院)，长沙 410008；3. 中南大学湘雅医院骨与关节代谢病医学中心，长沙 410008]

[摘 要] 目的：骨肉瘤(osteosarcoma，OS)是好发于青少年的恶性骨肿瘤，因其早期转移倾向和化疗耐药性，患者远期生存水平长期未见明显提高，亟需探索新的分子靶点和治疗策略。铁死亡作为一种铁依赖性脂质过氧化驱动的程序性细胞死亡形式，为攻克耐药性肿瘤提供了新的方向。ATP结合盒亚家族成员B6(ATP-binding cassette subfamily B member 6，*ABCB6*)隶属于ATP结合盒(ATP-binding cassette，ABC)转运蛋白超家族，主要定位于线粒体外膜，参与血红素合成与铁离子胞内转运。近年来研究提示*ABCB6*在多种肿瘤中异常表达并调控肿瘤恶性进展，但其在OS中的作用及机制尚不明确。本研究旨在系统阐明*ABCB6*在OS中的表达特征、临床预后意义及生物学功能，深入探究*ABCB6*调控OS铁死亡的分子机制，以期为由*ABCB6*介导的OS靶向治疗提供理论依据。**方法：**采用人OS细胞系HOS和143B及人骨髓间充质干细胞(bone marrow mesenchymal stem cells，BMSCs)作为研究对象。通过慢病毒介导的RNA干扰技术建立*ABCB6*稳定敲减的OS细胞株，并利用缺氧诱导因子1α(hypoxia-inducible factor 1-alpha，*HIF1A*)过表达慢病毒进行回补实验。通过细胞计数试剂盒-8(cell counting kit-8，CCK-8)增殖实验、平板克隆形成实验评估细胞增殖能力；Transwell小室迁移实验和划痕愈合实验检测细胞迁移能力；流式细胞术检测细胞凋亡。利用铁死亡相关表型实验探索*ABCB6*表达对OS铁死亡的影响。通过转录组测序分析差异表达基因及富集通路；染色质

©Journal of Central South University (Medical Science). All rights reserved.

免疫共沉淀和双荧光素酶报告基因实验验证HIF1A蛋白对谷胱甘肽过氧化物酶4(glutathione peroxidase 4，*GPX4*)启动子的直接结合与转录调控。采用铁螯合剂和蛋白酶体抑制剂干预以验证Fe^{2+}对HIF1A蛋白稳定性的调控。体内实验中，将*ABCB6*敲减及对照的143B细胞接种于裸鼠皮下，通过建立异种移植瘤模型评估*ABCB6*表达对OS体内生长的影响。**结果：***ABCB6*在OS细胞系中的信使RNA(messenger RNA，mRNA)和蛋白质表达水平均显著高于BMSCs(均*P*<0.05)，且TARGET(Therapeutically Applicable Research to Generate Effective Treatments)-OS队列分析显示*ABCB6*高表达组患者总生存期显著低于*ABCB6*低表达组[风险比(hazard ratio，*HR*)=2.94，95%置信区间(confidence interval，*CI*) 1.36~6.36，*P*<0.05]。*ABCB6*敲减显著抑制OS细胞增殖和克隆形成，降低迁移能力，增加细胞凋亡率，并伴随神经钙黏素(N-cadherin)下调和上皮钙黏素(E-cadherin)及活化型胱天蛋白酶-3(cleaved caspase-3)上调(均*P*<0.05)。*ABCB6*敲减使Liperfluo阳性细胞比例和二氢乙锭(dihydroethidium，DHE)氧化水平显著升高，胞内Fe^{2+}浓度增加，谷胱甘肽(glutathione，GSH)/氧化型谷胱甘肽(oxidized glutathione，GSSG)比值下降，线粒体膜电位降低，电镜下可见线粒体萎缩、嵴减少等典型铁死亡形态学改变；铁死亡抑制剂可逆转上述氧化应激变化(均*P*<0.05)。*ABCB6*敲减下调GPX4蛋白和mRNA水平(均*P*<0.05)，但对溶质载体家族7成员11(solute carrier family 7 member 11，SLC7A11)无显著影响(*P*>0.05)。转录组测序及京都基因和基因组数据库(Kyoto Encyclopedia of Genes and Genomes，KEGG)富集分析显示HIF-1信号通路在对照组中显著富集(*P*<0.001)；*ABCB6*敲减使HIF1A蛋白表达降低，而铁螯合剂和蛋白酶体抑制剂处理可分别通过螯合Fe^{2+}和抑制泛素-蛋白酶体途径逆转该降解过程(均*P*<0.05)。染色质免疫共沉淀结合定量聚合酶链反应(chromatin immunoprecipitation followed by quantitative polymerase chain reaction，ChIP-qPCR)和双荧光素酶报告基因实验证实HIF1A可直接结合*GPX4*启动子并激活其转录。在*ABCB6*敲减细胞中过表达*HIF1A*可恢复GPX4表达，并显著逆转*ABCB6*敲减所导致的增殖抑制、迁移能力下降和凋亡增加，同时恢复线粒体膜电位(均*P*<0.05)。裸鼠异种移植瘤实验表明，*ABCB6*敲减组的肿瘤体积和瘤重均显著小于对照组(均*P*<0.05)；免疫组织化学染色证实*ABCB6*敲减组中HIF1A和GPX4表达下调，Ki-67和N-cadherin阳性率降低，cleaved caspase-3和E-cadherin阳性率升高(均*P*<0.05)。**结论：**本研究首次系统揭示了*ABCB6*在OS中的致癌功能和预后预测价值，阐明了“*ABCB6*/Fe^{2+}/*HIF1A*/*GPX4*”信号轴调控OS铁死亡的完整分子机制。本研究不仅为OS的分子分型和预后评估提供了新的生物标志物，也为靶向*ABCB6*/*HIF1A*/*GPX4*轴诱导铁死亡的治疗策略奠定了理论基础。后续可进一步探索*ABCB6*上游调控机制及其在OS化疗耐药逆转中的潜在应用价值。

[关键词] 骨肉瘤；*ABCB6*；铁死亡；*HIF1A*；*GPX4*

Osteosarcoma (OS) is the most common primary bone malignancy, highly aggressive and metastatic, peaking in adolescents and children[1-2]. The global annual incidence is 2－3 per million[2]. Standard therapy, including surgical resection plus neoadjuvant/adjuvant chemotherapy, has improved localized disease 5-year survival to 60%−70%, but metastatic/recurrent OS has a poor 5-year survival of 20%−30%[1-2]. Genetic exploration is crucial for improving OS treatment[3-4]; however, the tumor's genetic complexity and instability hinder mechanistic studies and therapy development, highlighting the need to define oncogene and tumor suppressor roles in OS pathogenesis[3-4].

The human ATP-binding cassette (ABC) transporter superfamily comprises 48 genes in 7 subfamilies, many aberrantly expressed in cancers and linked to progression, drug resistance, and prognosis[5]. Recent studies[6-9] have indicated that ABC subfamily B member 6 (*ABCB6*) is associated with poor clinical outcomes and drug resistance in various cancers. Moreover, *ABCB6* mediates ferroptosis, and modulating its expression can induce ferroptosis to suppress tumor progression[10-11]. However, the role and mechanism of *ABCB6* in OS remain unexplored, warranting further investigation.

Ferroptosis is iron-dependent lipid peroxide-driven cell death with tumor-suppressive functions[12-14]. Hypoxia-inducible factor 1-alpha (*HIF1A*) promotes ferroptosis resistance in solid tumors and its silencing sensitizes tumors to ferroptosis inducers, suggesting that targeting *HIF1A* can modulate ferroptosis[15-16]. *HIF1A* undergoes proteasomal degradation regulated by prolyl hydroxylases (PHDs) and the von Hippel-Lindau protein (pVHL), with O_2 and Fe^{2+} serving as essential cofactors[17-19]. Notably, *ABCB6* maintains iron homeostasis, which is key for both HIF1A protein degradation and ferroptosis[20-22].

Herein, we identified *ABCB6* as an oncogene in OS via functional assays after *ABCB6* silencing. Subsequent experiments revealed that ferroptosis underlies the anti-

©Journal of Central South University (Medical Science). All rights reserved.

OS effects of *ABCB6* knockdown. Mechanistically, *ABCB6* silencing elevated intracellular Fe^{2+}, leading to HIF1A protein degradation and ferroptosis induction. Increased HIF1A protein degradation further reduced glutathione peroxidase 4 (*GPX4*) transcription, enhancing ferroptosis in OS cells. Together, these findings show that *ABCB6* acts as an oncogene and that targeting *ABCB6* induces ferroptosis to suppress OS progression, offering new insights for OS research and therapy.

1 Materials and methods

1.1 Ethics statements

The animal experiments in this study acquired approval from the Animal Care and Ethics Committee of Xiangya Hospital, Central South University (Approval number: 2023040746).

1.2 Cells, reagents, and transfection

Human bone marrow mesenchymal stem cells (BMSCs) were isolated from patients undergoing hip replacement at the Department of Orthopedics, Xiangya Hospital with informed consent.

The human OS cell lines, HOS and 143B cells, and 293T cells were purchased from Procell Company (WuHan, China). Under the circumstance of 5% CO_2 and 37 ℃, cells were cultured in Dulbecco's modified Eagle medium (DMEM; Biological Industries, Israel) added with 1% penicillin/streptomycin (Gibco, USA) and 10% fetal bovine serum (Gibco, USA). To minimize potential off-target effects, 2 independent short hairpin RNA (shRNA) sequences targeting *ABCB6* (SH1 and SH2) and their respective scrambled control lentiviruses were purchased from General Biosystems (Nanjing, China) and used for gene silencing. Lentiviruses for *HIF1A* overexpression and its empty-vector control were sourced from Genechem (Shanghai, China). *HIF1A* and *GPX4* plasmids for dual-luciferase assays were also synthesized by General Biosystems (Nanjing, China). *ABCB6*-silenced and *HIF1A*-overexpressed OS cells were established via lentiviral infection and selected with puromycin (1.2 mg/mL) for 4 weeks.

The following antibodies were used: anti-ABCB6 (121438, zenbio), anti-HIF1A (ab308433, ABclonal), anti-solute carrier family 7 member 11 (SLC7A11; 26864-1-AP, proteintech), anti-E-cadherin (ab40772, ABclonal), anti-N-cadherin (ab76011, ABclonal), anti-Ki-67 (ab15580, ABclonal), anti-GPX4 (30388-1-AP, proteintech), anti-cleaved caspase-3 (341034, zenbio), and anti-glyceraldehyde-3-phosphate dehydrogenase (GAPDH; 10494-1-AP, proteintech). Ferrostatin-1 (Fer-1; a lipid peroxidation scavenger), deferoxamine (DFO; an iron chelator), and MG-132 (a proteasome inhibitor) were purchased from MedChemExpress (MCE, USA) with the respective catalog numbers 347174-05-4, 138-14-7, and 133407-82-6.

1.3 Cancer Genome Atlas Program data acquisition and processing

The RNA sequencing and the corresponding clinical traits of 85 OS patients were downloaded from Therapeutically Applicable Research to Generate Effective Treatments (TARGET), acquiring from The Cancer Genome Atlas Program (TCGA) website (https://www.cancer. gov/ccg/research/genome-sequencing/tcga). The R package maxstat (Maximally Selected Rank Statistics with several *P*-value approximations, version 0.7−25.0) was utilized to compute the optimal cut-off value for ABCB6. The minimum group sample size was set to >25% and the maximum group sample size to <75% of the total sample. The resulting optimal cut-off value was 0.26. Based on this cut-off, patients were divided into a high-expressed group and a low-expressed group. Subsequently, we analyzed the prognostic difference between the 2 groups using the survfit function from the R package survival and assessed the statistical significance of the difference using the log-rank test. The data acquisition and utilization were in accordance in the policy of TCGA website.

1.4 Immunohistochemistry staining of tissues

For immunohistochemistry (IHC), tumor tissues were undergone fixation, permeabilization, dehydration, embedding, and section. Subsequently, tissue slides were incubated with anti-ABCB6, anti-Ki-67, anti-E-cadherin, anti-N-cadherin, anti-caspase-3, anti-HIF1A, anti-GPX4 primary and the corresponding secondary antibodies, and the details of IHC assays were performed as described in our previous study[23].

©Journal of Central South University (Medical Science). All rights reserved.

1.5 RNA extraction and real-time polymerase chain reaction

The total RNA was extracted from human BMSCs and OS cells using the AG RNAex Pro RNA extraction kit (AG, Changsha, China) and then utilized for the synthesis of complementary DNA (cDNA) using the Reverse Transcription kit (AG, Changsha, China). The TBGreen Premix Pro Taq HS real-time polymerase chain reaction (qPCR) kit (AG, Changsha, China) was utilized for qPCR analysis. The ΔΔCq method was utilized to calculate the relative RNA expression of each sample and the results were expressed as $2^{-\Delta\Delta Cq}$. *GAPDH* was used as the internal control gene. The primers for qPCR are shown in the Table 1.

Table 1 Primers for qPCR

Genes	Forward primer (5' to 3')	Reverse primer (5' to 3')
ABCB6	GGCTCTGGGGACTCTGG	CACGTAGGGAGAGATGCGA
HIF1A	AAGCACAGTTACAGTATTCCAGCAG	TCATCAGTGGTGGCAGTGGTAG
GPX4	AGAGATCAAAGAGTTCGCCGC	TCTTCATCCACTTCCACAGCG
GAPDH	GATTCCACCCATGGCAAATTC	CTGGAAGATGGTGATGGGATT

qPCR: Real-time polymerase chain reaction; *ABCB6*: ATP-binding cassette subfamily B member 6; *HIF1A*: Hypoxia-inducible factor 1-alpha; *GPX4*: Glutathione peroxidase 4; *GAPDH*: Glyceraldehyde-3-phosphate dehydrogenase.

1.6 Western blotting

Proteins were extracted with a mammalian total protein extraction kit (DE101-01, TransGen), resolved by 10% sodium dodecyl sulfate-polyacrylamide gel electrophoresis (SDS-PAGE), and transferred to polyvinylidene fluoride (PVDF) membranes. After blocking with 5% non-fat milk for 1 hour, membranes were incubated with primary antibodies overnight at 4 ℃, followed by secondary antibodies for 1 hour, and detected using an enhanced chemiluminescence (ECL) kit (BL520A, Biosharp, China). Of note, for mechanistic exploration of the signaling axis, cells were treated with 100 μmol/L DFO for 24 hours to chelate intracellular Fe^{2+}, and cells were exposed to 10 μmol/L MG-132 for 6 hours to evaluate the potential proteasomal degradation of HIF1A.

1.7 Cell proliferation and colony formation

Proliferation was evaluated using a cell counting kit (CCK)-8 (Beyotime, China). About 3 000 cells/well were seeded in 96-well plates and processed according the manufacturer's instructions. For colony formation, 500 cells/well were seeded in 6-well plates and cultured for 2 weeks as previously described[23].

1.8 Transwell migration and scratch wound-healing assay

Transwell migration assays were performed by seeding 2×10^4 cells in 200 μL serum-free medium into the upper chamber (24-well insert, Corning) with 800 μL complete medium below. For scratch assays, 3×10^5 cells were seeded in 6-well plates, scratched with a 1 mL tip at 90% confluence. Detailed procedures followed our previous study[23].

1.9 Flow cytometry

In term of cell apoptosis assay, cells were digested using ethylene diamine tetraacetic acid (EDTA) -free trypsin, washed twice with pre-cooled phosphate buffered saline (PBS), and stained with the apoptosis detection kit (#FXP023, 4A BIOTECH, China). Subsequently, the stained samples were incubated in the dark 10 min at room temperature and analyzed by flow cytometry within 1 hour.

For liperfluo and reactive oxygen species (ROS) analyses, OS cells were seeded in the 6-well plates and stained with liperfluo (Dojindo, Kumamoto, Japan) and dihydroethidium (DHE; US Everbright, Suzhou) probe in accordance to the manufacturer's protocol. Subsequently, the stained cells were digested with trypsin, washed twice with pre-cooled PBS and detected by flow cytometry. In the ferroptosis rescue experiments, cells were co-incubated with either 1 μmol/L Fer-1 or 100 μmol/L DFO for 24 hours, in order to assess the reversal of *ABCB6*-driven cell death and lipid peroxidation.

©Journal of Central South University (Medical Science). All rights reserved.

1.10 Detection of intracellular Fe^{2+} levels

Cells were cultured in the 24-well plate and then stained in 1 μmol/L FerroOrange (Dojindo, Kumamoto, Japan) diluted with Hank's Balanced Salt Solution for exactly 30 min under the circumstance of 5% CO_2 and 37 ℃. After staining, cells were imaged with a fluorescence microscope (Leica, Weztlar, German). Additionally, DFO (100 μmol/L, 24 hours) was employed to reverse the elevation of intracellular Fe^{2+} caused by *ABCB6* knockdown.

1.11 Detection of glutathione and oxidized glutathione

Cells were seeded in the 6-well plate, made into the lysates, and centrifuged at 10 000 ×*g* at 4 ℃ for 10 min. Subsequently, the supernatant was collected, and the total glutathione (GSH) and oxidized glutathione (GSSG) levels were determined using GSH and GSSG Assay Kit (Beyotime, Jiangsu, China). The operation and measurement of this assay were in accordance with the manufacturer's instructions.

1.12 Mitochondrial membrane potential detection

Since ferroptotic cells typically display decreased mitochondrial membrane potential (MMP), we employed the 5,5',6,6'-tetrachloro-1,1',3,3'-tetraethyl-imidacarbocyanine iodide (JC-1) probe to detect MMP changes after *ABCB6* knockdown. MMP was conducted using JC-1 MMP Assay Kit (Solarbio, Beijing, China). Cells were seeded in the 24-well plate. After cultured overnight, cells were stained with 1×JC-1 solution for 20 min in the dark and then imaged with a fluorescent microscope (Leica, Weztlar, German). JC-1 images were analyzed with ImageJ (Fiji). For each field, the mean fluorescence intensities of green (JC-1 monomer) and red (JC-1 aggregate) were measured after manually outlining regions of interest (ROI). The red/green ratio was calculated to reflect mitochondrial membrane potential.

1.13 Transmission electron microscope

Cells in 10 cm dishes were fixed with 2.5% glutaraldehyde for 5 min, scraped, and centrifuged. The pellet was fixed again in the dark for 30 min, post-fixed with 1% osmium tetroxide, dehydrated in ethanol and acetone, infiltrated with epoxy resin overnight, embedded, and polymerized at 60 ℃ for 48 hours. Sections were cut with an ultra-microtome (Leica EM UC7), stained with uranyl acetate and lead citrate, and observed by transmission electron microscope (TEM; Talos L120C G2) at 120 keV.

1.14 Transcriptome sequencing

Total RNA was extracted from *ABCB6*-silenced and control OS cells using TRIzol reagent (AG, Changsha, China) according to the manufacturer's protocol. Transcriptome sequencing and analysis were performed by OE Biotech (Shanghai, China). Differential expression analysis (DEA) was conducted using DESeq2, with significantly differentially expressed genes (DEGs) defined as Q value<0.05 and fold change >2 or <0.5.

1.15 Chromatin immunoprecipitation and dual-luciferase assays

Chromatin immunoprecipitation (ChIP) assays were performed using a ChIP kit (Bersinbio, Guangzhou) in 143B and HOS cells according the manufacturer's protocol. Immunoprecipitation used an anti-HIF1A antibody, with normal immunoglobulin (Ig) G as negative control and input chromatin as normalization control. Purified DNA was analyzed by qPCR, and data were presented as percentage of input. The primers are listed in Table 2.

Table 2 Primers for ChIP-qPCR

Target region	Forward primer (5' to 3')	Reverse primer (5' to 3')
GPX4 promoter region	AAAGGTAAATAAGAGTTGGGGACAC	AAGAAGGCGGGGAAGGG

ChIP: Chromatin immunoprecipitation.

©Journal of Central South University (Medical Science). All rights reserved.

The dual-luciferase assay was performed using Luc-Pair™ Duo Luciferase HS Assay Kit (GeneCopoeia, Guangzhou, China). In brief, 293T cells were seeded in the 12-well plates and infected with the constructed luciferase reporter plasmid. After infected 48 hours, the cells were lysised and used for fluorescence detection in accordance with the manufacturer's instructions.

1.16 Xenograft mouse models and in-situ tumor formation

For xenograft mouse models, 4- to 6-week-old female nude mice were randomly divided into the *ABCB6*-knockdown and the negative control groups (n=5), and the corresponding 143B OS cells were injected in these mice. In the subsequent feeding days, the tumor volumes of mice were measured every 5 days, and tumors were harvested after 25 days, with their weights measured.

1.17 Statistical analysis

The quantitative data were expressed as the mean± standard deviation and tested by unpaired student's t-test. GraphPad Prism 8 were utilized for data processing, statistical analysis, and presentation of all the experimental results. The indicated P value was considered statistically significant.

2 Results

2.1 *ABCB6* expression was associated with OS patients' prognoses

Compared with human BMSCs, the messenger RNA (mRNA) levels of *ABCB6* were elevated in OS cells, particularly in HOS and 143B cells (both P<0.05, Figure 1A). Consistently, western blotting analysis confirmed that ABCB6 protein expression was also higher in OS cells than in BMSCs (P<0.05, Figure 1B). Subsequently, the TARGET-OS cohort was used to investigate the clinical significance of *ABCB6* upregulation in OS and the Kaplan-Meier curve revealed that high *ABCB6* mRNA expression was negatively associated with the prognosis of OS patients [hazard ratio (*HR*)=2.94, 95% confidence interval (*CI*) 1.36 to 6.36, P<0.05; Figure 1C]. To further assess the functional role of *ABCB6* in OS progression, we knocked down *ABCB6* expression in 143B and HOS cells (both P<0.05, Figure 1D). Transwell migration and scratch wound-healing assays demonstrated that *ABCB6* knockdown significantly impaired the migratory capacity of OS cells (both P<0.05, Figure 1E and 1F). Meanwhile, flow cytometry analysis of cell apoptosis revealed that *ABCB6* silencing markedly increased the apoptosis rate of OS cells (P<0.05, Figure 2A). Furthermore, we examined the effect of *ABCB6* on OS cell proliferation. The results showed that reduced *ABCB6* expression suppressed cell proliferation and colony formation, ultimately inhibiting OS growth (both P<0.05, Figure 2B and 2C). Finally, western blotting of apoptosis- and migration-related markers indicated that *ABCB6* knockdown markedly decreased N-cadherin expression while increasing both E-cadherin and cleaved caspase-3 levels, suggesting that *ABCB6* silencing promotes apoptosis and inhibits migration in OS cells (all P<0.05, Figure 2D). Taken together, these findings indicate that *ABCB6* functions as an oncogene in OS, and its elevated expression correlates with a worse prognosis in OS patients.

2.2 Targeting *ABCB6* induced OS cells *GPX4*-associated ferroptosis

First, the liperfluo assay, a specific indicator of ferroptosis, revealed that *ABCB6* silencing significantly increased the proportion of liperfluo-positive cells, indicating the occurrence of ferroptosis (Figure 3A). Meanwhile, the DHE probe, used to assess cellular oxidation levels, showed that *ABCB6*-knockdown OS cells exhibited higher oxidation levels compared with controls (Figure 3B). The detection results of intracellular Fe^{2+} concentration demonstrated that *ABCB6* silencing increased the intracellular Fe^{2+} concentration (Figure 3C). In contrast to the elevated oxidation level, the level of reducing substances, such as GSH/GSSG, decreased following *ABCB6* knockdown (P<0.05, Figure 3D). The results of the JC-1 experiment showed that *ABCB6* silencing reduced the MMP of OS cells, suggesting mitochondrial damage (P<0.05, Figure 3E). The results of the TEM examination further confirmed revealed damaged mitochondrial structures in *ABCB6*-knockdown OS cells (Figure 4A and 4B). Moreover, treatment with ferroptosis inhibitors reversed the elevated oxidation levels induced by *ABCB6* silencing, further supporting the involvement of ferroptosis (Figure 4C and 4D). Western blotting analysis revealed that GPX4 expression was

©Journal of Central South University (Medical Science). All rights reserved.

significantly reduced following *ABCB6* knockdown ($P<0.05$), whereas SLC7A11 expression showed no significant change ($P>0.05$, Figure 4E). Additionally, qPCR analysis demonstrated that the mRNA levels of *GPX4* were also downregulated upon *ABCB6* silencing, indicating that *ABCB6* regulates *GPX4* expression at the transcriptional level (all $P<0.05$, Figure 4F and 4G). Taken together, these findings suggest that the anti-OS effect of *ABCB6* knockdown likely stems from its induction of *GPX4*-associated ferroptosis in OS cells.

2.3 *ABCB6* silencing induced OS ferroptosis via Fe^{2+}/*HIF1A*/*GPX4* signaling pathway

To further elucidate the mechanism by which *ABCB6* regulates *GPX4* expression, we performed transcriptome sequencing (Figure 5A). Gene Ontology (GO) analysis revealed that DEGs were enriched in transcriptional pathways, including positive regulation of transcription by RNA polymerase II and DNA binding, suggesting that *ABCB6* may affect transcriptional activity in OS cells (Figure 5B). Moreover, the HIF-1 signaling pathway was significantly enriched in the negative control group ($P<0.001$, Figure 6A), and subsequent western blotting confirmed that *ABCB6* knockdown decreased HIF1A protein levels (both $P<0.05$, Figure 6B). Fe^{2+} probe assays confirmed that DFO treatment reversed the *ABCB6* knockdown-induced elevation of intracellular Fe^{2+} (Figure 6C), and western blotting showed that DFO also reversed the degradation of HIF1A (both $P<0.05$, Figure 6D). Subsequently, we employed a ubiquitination inhibitor to block HIF1A degradation. Western blotting analysis revealed that the inhibitor attenuated the degradation of HIF1A protein (both $P<0.05$, Figure 6E), indicating that *ABCB6* likely promotes HIF1A protein degradation through elevated intracellular Fe^{2+} concentration.

ChIP-qPCR assays results showed significant enrichment of the *GPX4* promoter region in anti-HIF1A immunoprecipitates compared with the IgG control (Figure 7A). Dual luciferase reporter assays further confirmed that HIF1A promotes *GPX4* transcription (Figure 7B). Consistently, western blotting showed that *ABCB6* knockdown reduced HIF1A expression and subsequently suppressed GPX4 expression (all $P<0.05$, Figure 7C). To validate whether the *ABCB6* knockdown-induced downregulation of GPX4 is mediated by HIF1A, we overexpressed *HIF1A* in *ABCB6*-silenced cells, the results showed that *HIF1A* overexpression reversed the GPX4 downregulation caused by *ABCB6* knockdown (all $P<0.05$, Figure 7D and 7E).

CCK-8 assays demonstrated that *HIF1A* overexpression rescued the proliferative ability suppressed by *ABCB6* knockdown (Figure 8A and 8B). Transwell assays showed that *HIF1A* overexpression enhanced the migration of *ABCB6*-silenced OS cells (Figure 8C and 8D). Furthermore, *HIF1A* overexpression significantly inhibited apoptosis in *ABCB6*-knockdown OS cells (Figure 8E). In addition, MMP was increased upon *HIF1A* overexpression, indicating that HIF1A alleviates mitochondrial damage induced by *ABCB6* silencing (Figure 8F).

Taken together, our study demonstrates that *ABCB6* silencing induces *GPX4*-related ferroptosis in OS cells via the Fe^{2+}/*HIF1A* signaling pathway, thereby inhibiting OS progression.

2.4 *ABCB6* knockdown suppressed OS growth in vivo

Xenograft tumor formation assay results showed that tumors derived from *ABCB6*-silenced stable cells exhibited significantly reduced volume and weight compared with the negative control group (both $P<0.05$, Figure 9A－9C). IHC staining for ABCB6 confirmed successful knockdown of *ABCB6* in the sh*ABCB6* groups (Figure 9D). Meanwhile, IHC analysis of tumor sections revealed that, compared with the negative control group, the expression levels of HIF1A and GPX4 were downregulated in the *ABCB6* knockdown groups (both $P<0.05$, Figure 9D－9F). Subsequently, we found that in the *ABCB6* knockdown groups, intratumoral cleaved caspase-3 levels were upregulated, whereas the expression of the proliferation marker Ki-67 was inhibited, compared with the negative control group (both $P<0.05$, Figure 9G－9I). Furthermore, IHC results revealed that E-cadherin expression was upregulated upon *ABCB6* knockdown, whereas N-cadherin expression showed the opposite trend (both $P<0.05$, Figure 9J － 9L). Collectively, our in vivo findings corroborated the in vitro results, demonstrating that *ABCB6* silencing suppresses OS progression by inducing *GPX4*-related ferroptosis in OS cells via the Fe^{2+}/*HIF1A* signaling pathway.

©Journal of Central South University (Medical Science). All rights reserved.

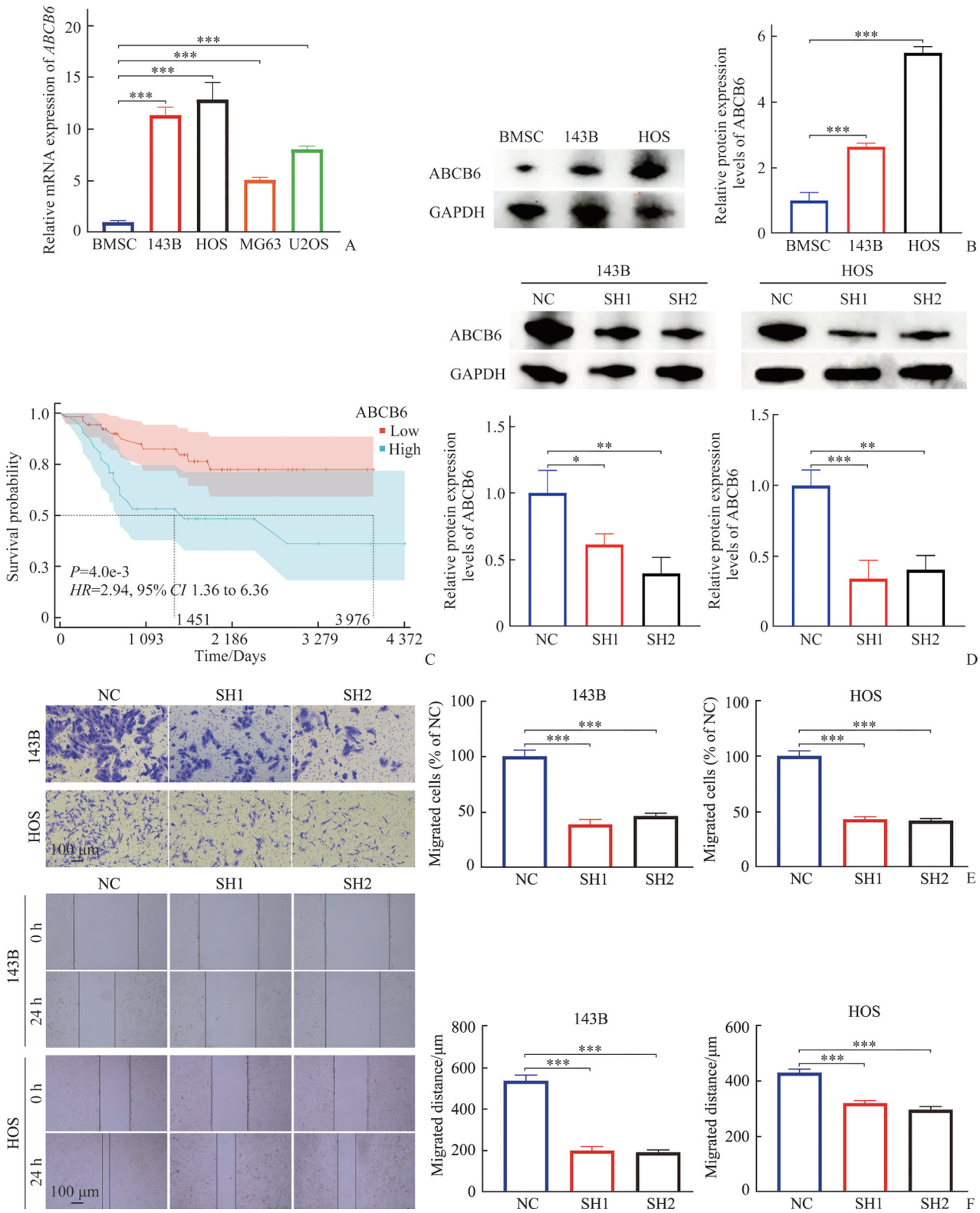

Figure 1 *ABCB6* functioned as an oncogene in OS, and its knockdown suppressed OS cell migration

A: The mRNA expression of *ABCB6* was upregulated in OS cells. B: Compared with BMSCs, the protein expression of ABCB6 was upregulated in OS cells, 143B and HOS cells. C: TARGET-OS cohort showed that *ABCB6* mRNA expression was negatively associated with the prognosis of OS patients. D: Validation of the knockdown efficiency of ABCB6 in OS cells. E: Transwell assay. F: Scratch wound-healing assay. The data represent the mean±standard deviation. **P*<0.05, ***P*<0.01, and ****P*<0.001 indicate a significant difference between the indicated groups. mRNA: Messenger RNA; *ABCB6*: ATP-binding cassette subfamily B member 6; OS: Osteosarcoma; BMSC: Bone marrow mesenchymal stem cell; TARGET: Therapeutically Applicable Research to Generate Effective Treatments; GAPDH: Glyceraldehyde-3-phosphate dehydrogenase; *HR*: Hazard ratio; *CI*: Confidence interval; NC: Negative control; OD: Optical density.

©Journal of Central South University (Medical Science). All rights reserved.

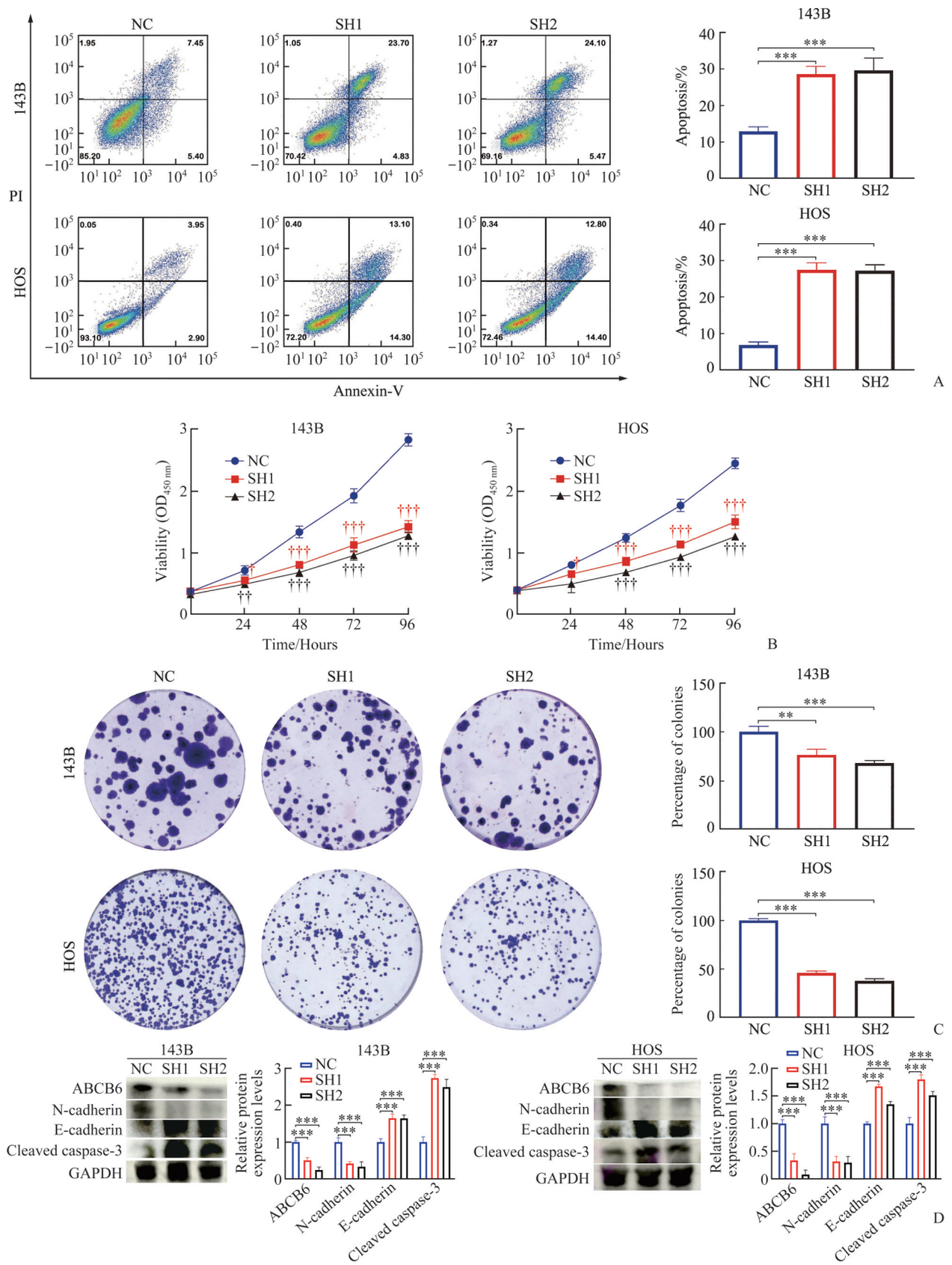

Figure 2 Knockdown of *ABCB6* promoted apoptosis and inhibited proliferation in OS cells

A: Cell apoptosis assay. B: CCK-8 assay, †P<0.05, ††P<0.01, and †††P<0.001 vs the NC group. C: Colony formation assay. D: Western blotting analysis revealed that *ABCB6* knockdown significantly reduced N-cadherin expression while concurrently upregulating E-cadherin and cleaved caspase-3 levels. The data represent the mean±standard deviation. *P<0.05, **P<0.01, and ***P<0.001 indicate a significant difference between the indicated groups. CCK-8: Cell counting kit-8; PI: Propidium iodide.

©Journal of Central South University (Medical Science). All rights reserved.

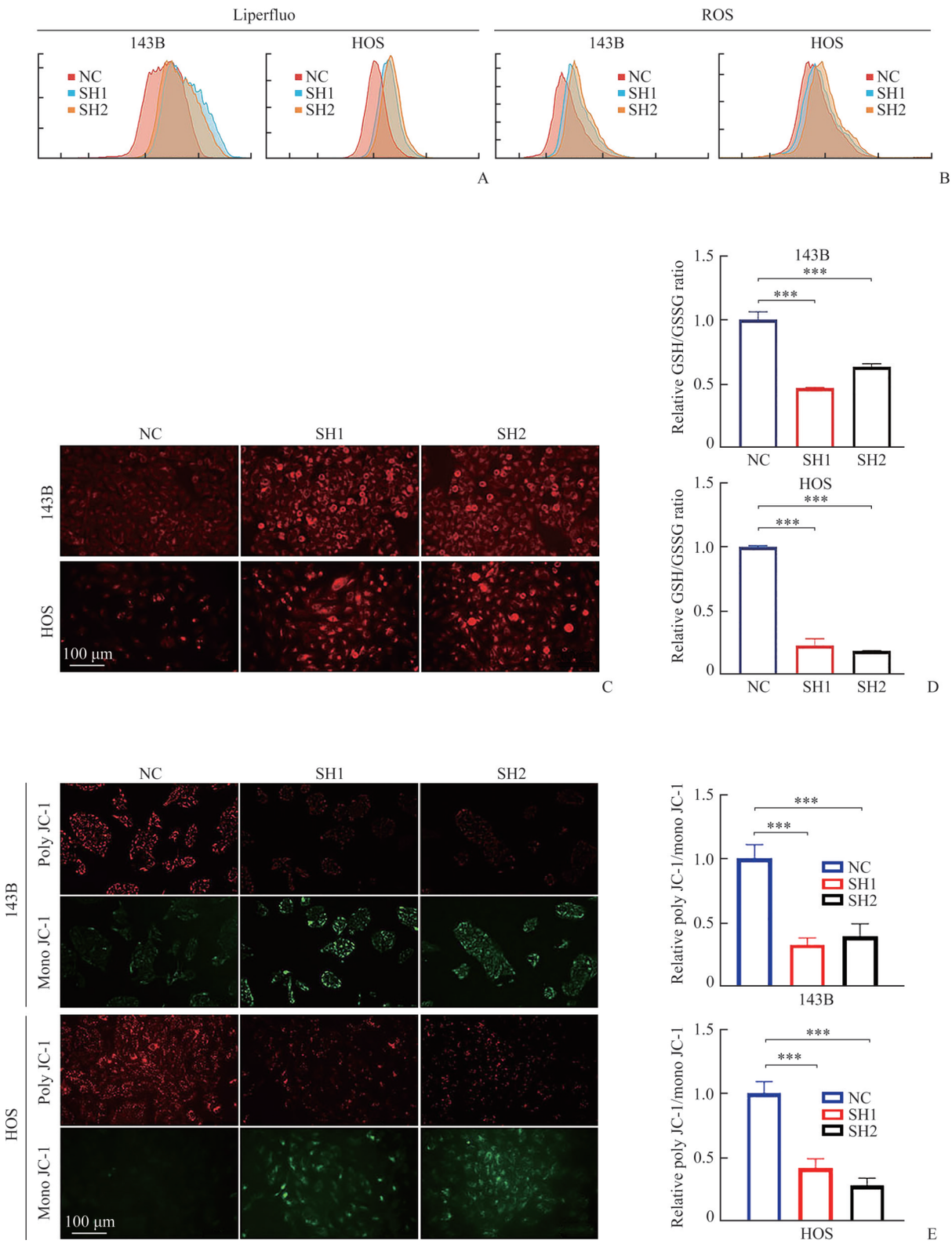

Figure 3 Knockdown of *ABCB6* induced oxidative stress, elevated Fe^{2+} levels, and reduced mitochondrial membrane potential in OS cells

A: Liperfluo assays. B: ROS detection. C: Intracellular Fe^{2+} concentration detection. D: GSH and GSSG detection. E: Mitochondrion membrane potential. The data represent the mean±standard deviation. **P*<0.05, ***P*<0.01, and ****P*<0.001 indicate a significant difference between the indicated groups. GSH: Glutathione; GSSG: Glutathione disulfide; ROS: Reactive oxygen species; JC-1: 5,5',6,6'-Tetrachloro-1,1',3,3'-tetraethylbenzimidazolylcarbocyanine iodide.

©Journal of Central South University (Medical Science). All rights reserved.

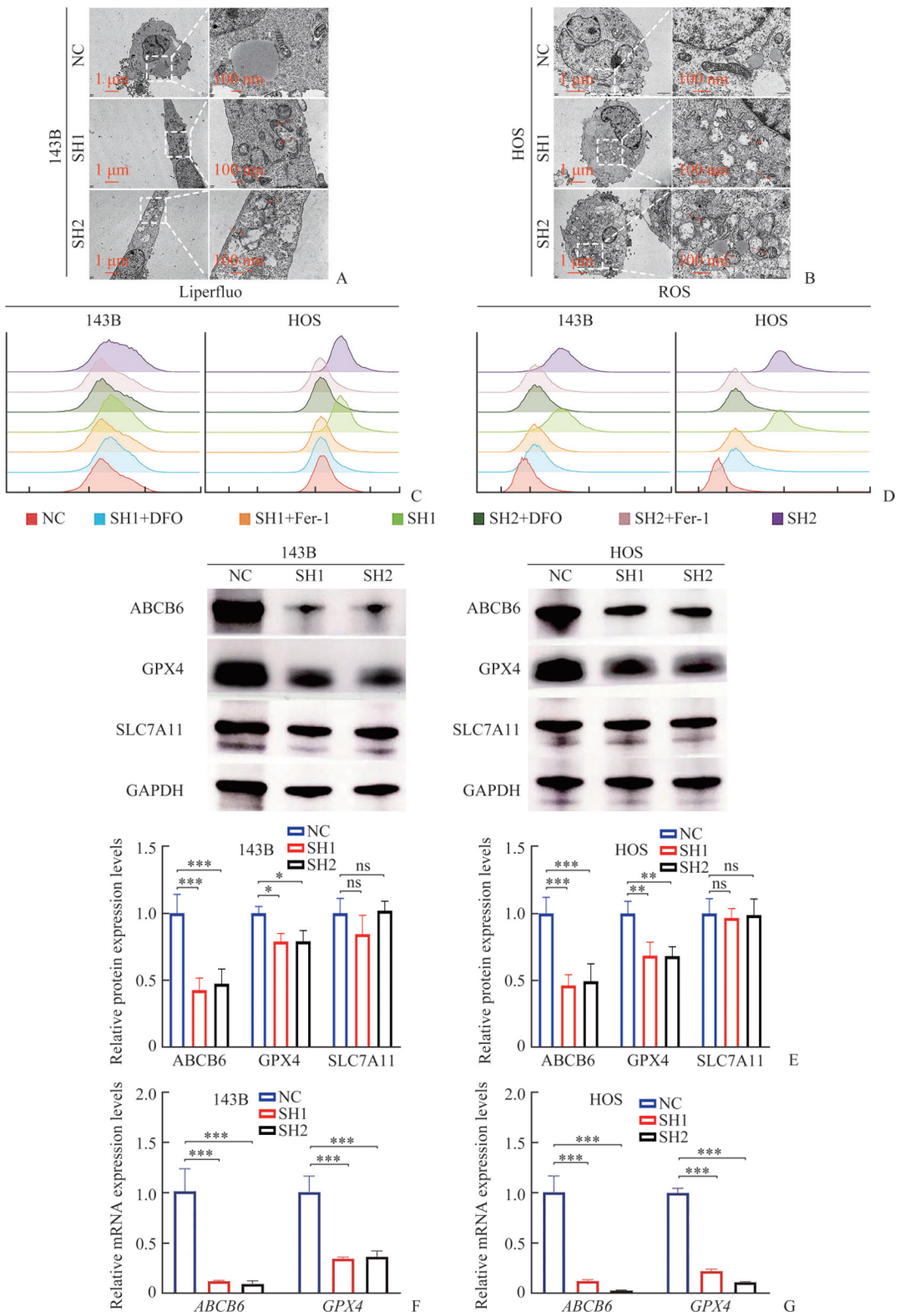

Figure 4 Ferroptosis inhibitor reversed *ABCB6* knockdown-induced oxidative stress in OS cells, and GPX4 served as a potential mediator of ABCB6 action

A and B: Transmission electron microscope revealed that *ABCB6* knockdown led to mitochondrial structural damage in 143B cells (A) and HOS cells (B). C and D: Ferroptosis inhibitors reversed the lipid peroxidation (C) and ROS (D) induced by *ABCB6* knockdown. E: Expressional exploration of ferroptosis related molecules. F and G: qPCR of *ABCB6* and *GPX4* in 143B cells (F) and HOS cells (G). The data represent the mean±standard deviation. **P*<0.05, ***P*<0.01, and ****P*<0.001 indicate a significant difference between the indicated groups. *SLC7A11*: Solute carrier family 7 member 11; *GPX4*: Glutathione peroxidase 4; qPCR: Real-time polymerase chain reaction.

©Journal of Central South University (Medical Science). All rights reserved.



Figure 5 Transcriptome sequencing revealed the transcriptional landscape of OS cells following *ABCB6* knockdown

A: Volcano plot shows the differentially expressed genes between the *ABCB6* knockdown group and the control group. B: Gene ontology analysis. *HIF1A*: Hypoxia-inducible factor 1-alpha; GSEA: Gene Set Enrichment Analysis.

©Journal of Central South University (Medical Science). All rights reserved.

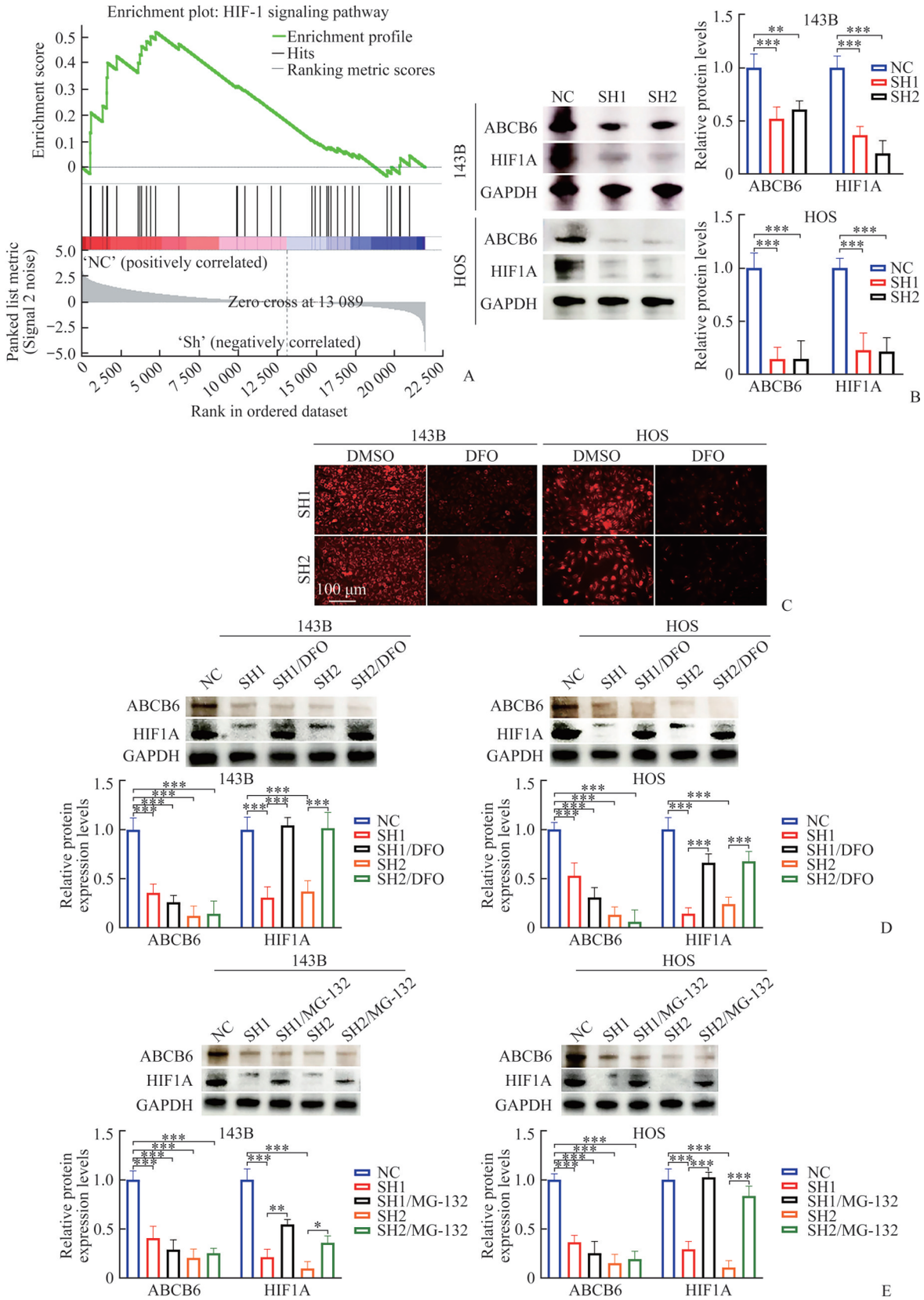

Figure 6 *ABCB6* knockdown inhibited HIF1A expression

A: GSEA analysis. B: Expressional exploration of HIF1A in *ABCB6* knockdown cells. C: DFO could reduce the elevated intracellular Fe^{2+} concentration resulted from *ABCB6* knockdown. D: DFO could reverse the degradation of HIF1A resulted from *ABCB6* knockdown. E: Proteasome inhibitor could reverse the degradation of HIF1A resulted from *ABCB6* knockdown. The data represent the mean±standard deviation. **P*<0.05, ***P*<0.01, and ****P*<0.001 indicate a significant difference between the indicated groups. FC: Fold change.

©Journal of Central South University (Medical Science). All rights reserved.

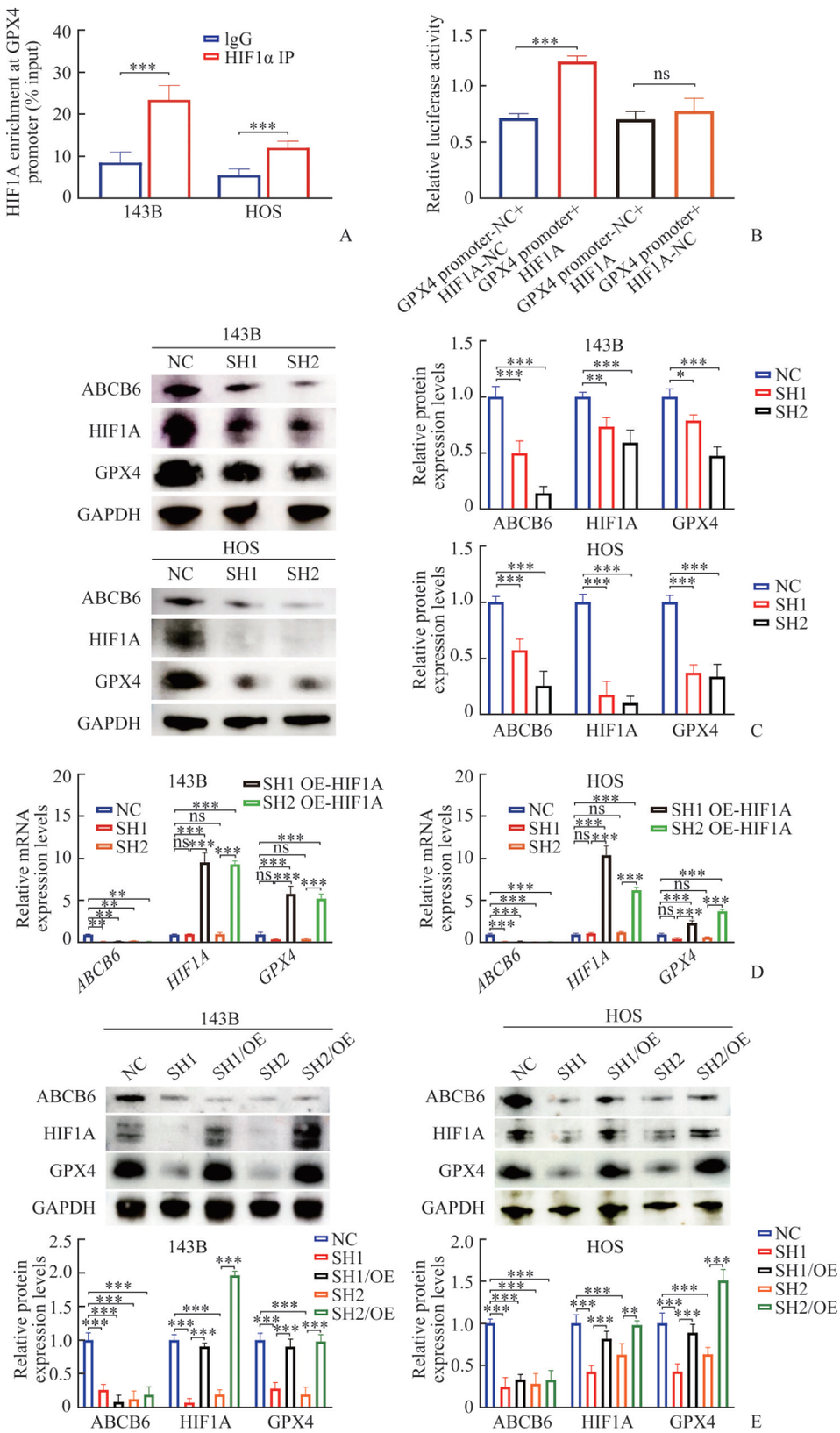

Figure 7 ***ABCB6* silencing induced OS ferroptosis via Fe^{2+}/*HIF1A*/*GPX4* signaling pathway**

A: ChIP-qPCR of HIF1A enrichment at the *GPX4* promoter. B: Dual-luciferase assay. C: Expressional exploration of HIF1A and GPX4 in *ABCB6* knockdown cells. D: qPCR indicated that *HIF1A* overexpression reversed the decreased GPX4 in *ABCB6* knockdown 143B cells and HOS cells. E: Western blotting indicated that HIF1A overexpression reversed the decreased GPX4 in *ABCB6* knockdown 143B cells and HOS cells. The data represent the mean±standard deviation. **P*<0.05, ***P*<0.01, and ****P*<0.001 indicate a significant difference between the indicated groups. ChIP: Chromatin immunoprecipitation; Ig: Immunoglobulin; OE: Over expression.

©Journal of Central South University (Medical Science). All rights reserved.

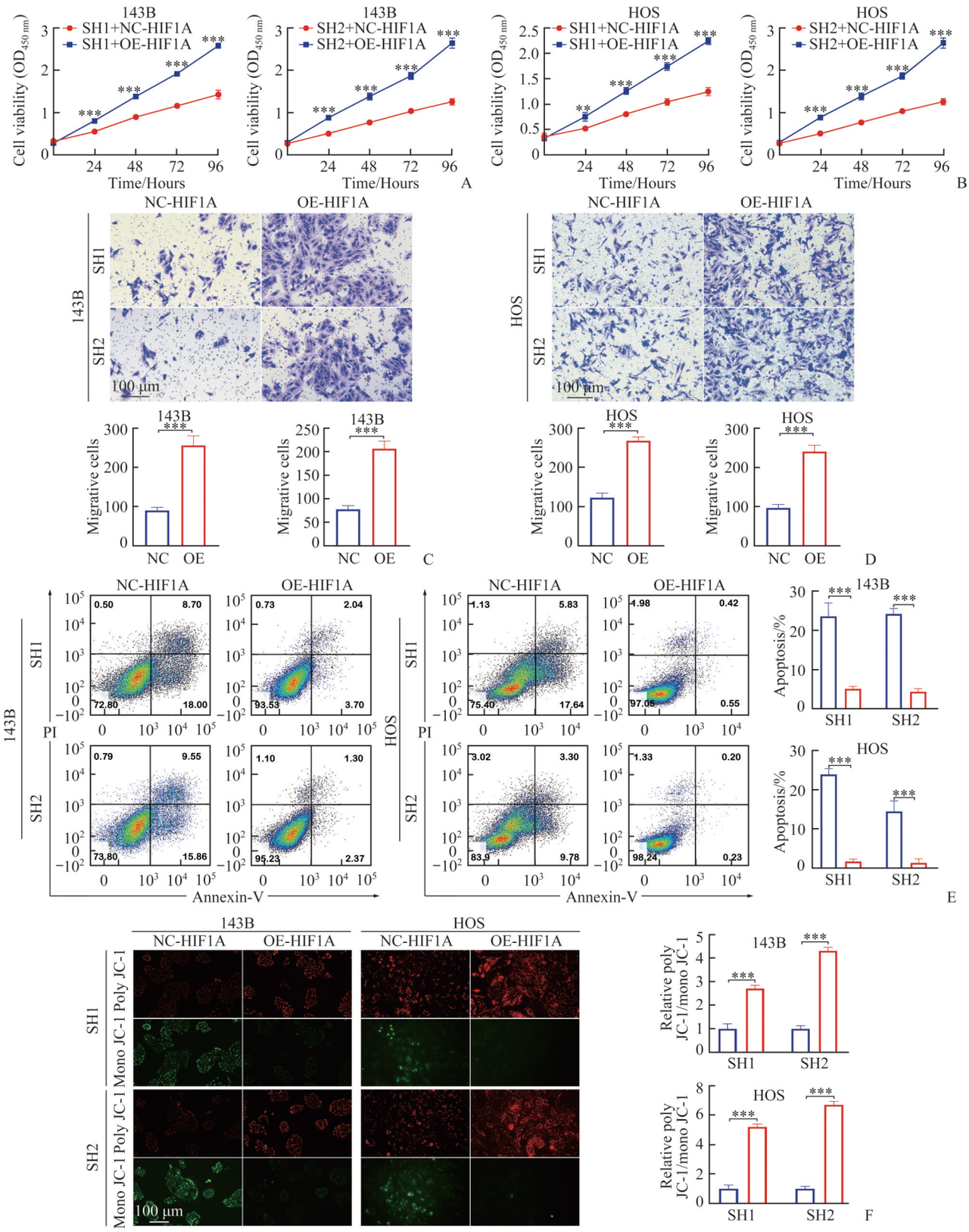

Figure 8 *HIF1A* overexpression reversed the biological functional inhibition in *ABCB6* knockdown cells

A and B: CCK-8 assays demonstrated that *HIF1A* overexpression reversed the proliferative inhibition in *ABCB6* knockdown 143B cells (A) and HOS cells (B). C and D: Transwell assays exhibited that *HIF1A* overexpression reversed the weaken migrative inhibition in *ABCB6* knockdown 143B cells (C) and HOS cells (D). E: Flow cytometry displayed that *HIF1A* overexpression reduced the apoptosis rate of 143B cells and HOS cells caused by *ABCB6* knockdown. F: *HIF1A* overexpression reversed the reduced MMP in *ABCB6* knockdown cells. The data represent the mean±standard deviation. **P*<0.05, ***P*<0.01, and ****P*<0.001 indicate a significant difference between the indicated groups.

©Journal of Central South University (Medical Science). All rights reserved.

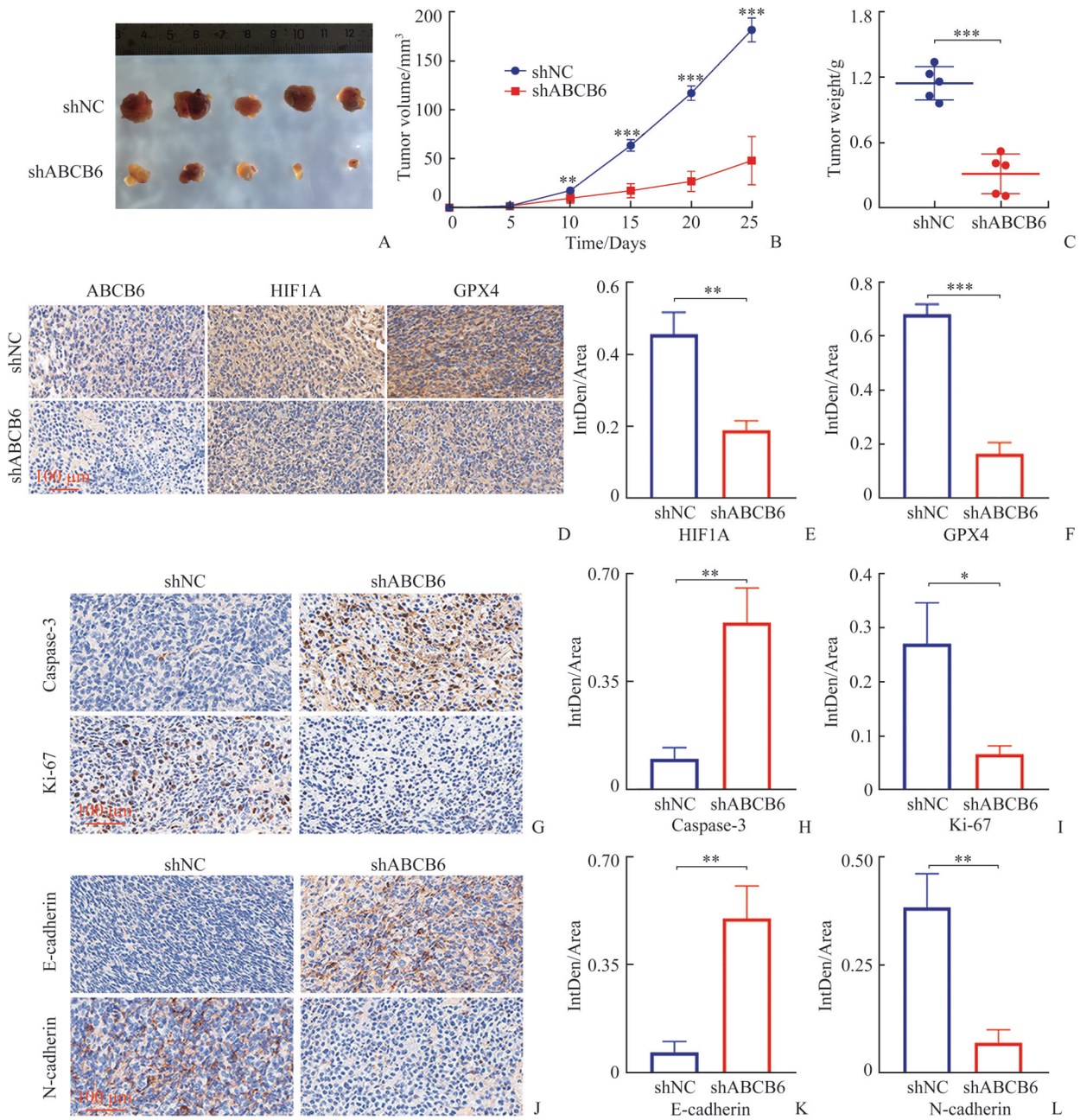

Figure 9 Validation of anti-OS effects of *ABCB6* in vivo

A: Ex vivo tumors showed that *ABCB6* knockdown inhibited the in vivo growth of OS. B: Tumor growth curves showed that tumor growth in the *ABCB6*-knockdown group was significantly inhibited compared with the control group. C: Tumor weight measurements revealed a significant difference between the *ABCB6*-knockdown group and the control group. D−F: IHC staining against HIF1A (D and E) and GPX4 (D and F). G−I: IHC staining against cleaved caspase-3 (G and H) and Ki-67 (G and I). J−L: IHC staining against E-cadherin (J and K) and N-cadherin (J and L). The data represent the mean±standard deviation. **P*<0.05, ***P*<0.01, and ****P*<0.001 indicate a significant difference between the indicated groups.

3 Discussion

The therapeutic bottleneck in OS necessitates exploring its molecular mechanisms to develop novel strategies[2-3, 24]. Since 2012, ferroptosis has been a promising approach for refractory cancers[12, 25-26]. Cancer cells resistant to conventional therapies often remain ferroptosis-susceptible, offering a complementary OS strategy[25, 27-28]. Inducing ferroptosis in OS may overcome resistance and immune non-

©Journal of Central South University (Medical Science). All rights reserved.

responsiveness[29-31], thus representing a potential avenue to break the therapeutic dilemma in OS.

In this study, we identified *ABCB6* as an oncogene in OS that is negatively associated with patient prognosis. *ABCB6* expression was upregulated in OS cell lines compared with hBMSCs, and Kaplan-Meier analysis of the TARGET-OS cohort revealed distinct prognoses between patients with differential *ABCB6* expression. Previous studies have implicated *ABCB6* in tumorigenesis, progression, and chemoresistance in various cancers[6, 32]; however, its role and mechanism in OS remain unexplored. Based on the differential expression and prognostic significance, we selected 2 OS cell lines with the highest *ABCB6* upregulation for further investigation. Functional assays demonstrated that *ABCB6* knockdown suppressed OS cell proliferation and migration while promoting apoptosis. We note that *ABCB6* knockdown simultaneously induces both ferroptosis and apoptosis in OS cells; however, the temporal relationship and molecular crosstalk between these 2 processes remain unclear. Future studies using time-sequential inhibition experiments, e. g., blocking key nodes of apoptosis or ferroptosis, are required to determine whether they occur sequentially or independently in parallel. Moreover, a xenograft tumor formation assay in nude mice confirmed the in vivo tumor-suppressive effect of *ABCB6* knockdown. Therefore, targeting *ABCB6* exhibits therapeutic potential for OS, and elucidating its molecular mechanism will facilitate clinical translation and treatment optimization.

Further mechanistic exploration revealed that the anti-OS effect of *ABCB6* knockdown may be attributed to its induction of ferroptosis. *ABCB6* silencing led to elevated oxidation levels, lipid peroxidation, and mitochondrial damage in OS cells; these effects were reversed by ferroptosis inhibitors, confirming that *ABCB6* silencing triggers ferroptosis. Previous studies have shown that *ABCB6* plays a role in regulating ferroptosis[10-11]. For instance, Yin, et al[11] reported that targeting *ABCB6* suppresses the *PI3K*/*AKT* pathway to induce ferroptosis in multiple myeloma cells. In our study, both mRNA and protein levels of the ferroptosis-related gene *GPX4* were significantly downregulated following *ABCB6* knockdown. Transcriptomic analysis revealed enrichment of DEGs in transcription-related pathways, suggesting that *ABCB6* knockdown may affect *GPX4* transcription. Notably, the HIF-1 signaling pathway was enriched in the negative control group. Given that HIF1A is a transcription factor for ferroptosis-related genes[33-35], we hypothesized that HIF1A mediates the effect of *ABCB6* knockdown on *GPX4* expression. ChIP and dual-luciferase assays confirmed that HIF1A binds to the *GPX4* promoter and promotes its transcription, which was further validated by western blotting. Hence, *ABCB6* may induce OS cell ferroptosis via the *HIF1A*/*GPX4* signaling pathway.

We found that *ABCB6* knockdown increased intracellular Fe^{2+} and downregulated the HIF-1 signaling pathway. Given that Fe^{2+} promotes HIF1A protein degradation[17-18, 36] and *ABCB6* regulates iron homeostasis[20-23, 25, 37], we hypothesized that elevated Fe^{2+} leads to HIF1A protein degradation. Treatment with the iron chelator DFO or the proteasome inhibitor MG-132 reversed this degradation, confirming the hypothesis. Furthermore, *HIF1A* overexpression in *ABCB6*-silenced OS cells rescued proliferation and migration while inhibiting apoptosis, indicating that the anti-OS effect of *ABCB6* knockdown partly depends on HIF1A protein degradation. Consistent with reports that *HIF1A* promotes ferroptosis resistance[15-16, 33, 38], *ABCB6* knockdown reduced HIF1A expression and MMP, both of which were restored by *HIF1A* overexpression. Notably, GPX4 expression consistently paralleled HIF1A under all conditions, and ChIP and dual-luciferase assays confirmed that HIF1A binds to and transcriptionally activates *GPX4*. Collectively, *ABCB6* silencing elevates intracellular Fe^{2+}, which promotes HIF1A protein degradation, thereby suppressing *GPX4* transcription and ultimately triggering ferroptosis in OS cells.

In summary, this study identifies *ABCB6* as an oncogene in OS, and targeting *ABCB6* exerts potent anti-OS effects by inducing ferroptosis. Mechanistically, *ABCB6* knockdown increases intracellular Fe^{2+} concentration, facilitating HIF1A protein degradation, which in turn suppresses *GPX4* transcription and expression, ultimately triggering ferroptosis in OS cells.

Contributions: LIN Zili Research design, carried out experiments, performed data statistics and analysis, wrote and revised the paper; LUO Hao and LI Xiangyao

©Journal of Central South University (Medical Science). All rights reserved.

Conducted the experiments, wrote the manuscript and made figure as well as table; LUO Wei Selected the topic and revised the manuscript. The final version of the manuscript has been approved and read by all authors.

Conflict of interest: The authors declare that they have no conflicts of interest to disclose.

References

[1] Gill J, Gorlick R. Advancing therapy for osteosarcoma[J]. Nat Rev Clin Oncol, 2021, 18(10): 609-624. https://doi.org/10.1038/s41571-021-00519-8.

[2] Meltzer PS, Helman LJ. New horizons in the treatment of osteosarcoma[J]. N Engl J Med, 2021, 385(22): 2066-2076. https://doi.org/10.1056/NEJMra2103423.

[3] Kansara M, Teng MW, Smyth MJ, et al. Translational biology of osteosarcoma[J]. Nat Rev Cancer, 2014, 14(11): 722-735. https://doi.org/10.1038/nrc3838.

[4] Truong DD, Weistuch C, Murgas KA, et al. Mapping the single-cell differentiation landscape of osteosarcoma[J]. Clin Cancer Res, 2024, 30(15): 3259-3272. https://doi.org/10.1158/1078-0432.CCR-24-0563.

[5] Sarkadi B, Homolya L, Szakács G, et al. Human multidrug resistance ABCB and ABCG transporters: participation in a chemoimmunity defense system[J]. Physiol Rev, 2006, 86(4): 1179-1236. https://doi.org/10.1152/physrev.00037.2005.

[6] Shibahara M, Kurita T, Murakami M, et al. Association of UBE2L6 and ABCB6 expression with platinum resistance in serous ovarian carcinoma[J]. Anticancer Res, 2023, 43(8): 3787-3792. https://doi.org/10.21873/anticanres.16564.

[7] Xiang L, Wang Y, Lan J, et al. HIF-1-dependent heme synthesis promotes gemcitabine resistance in human non-small cell lung cancers via enhanced ABCB6 expression[J]. Cell Mol Life Sci, 2022, 79(6): 343. https://doi.org/10.1007/s00018-022-04360-9.

[8] Polireddy K, Chavan H, Abdulkarim BA, et al. Functional significance of the ATP-binding cassette transporter B6 in hepatocellular carcinoma[J]. Mol Oncol, 2011, 5(5): 410-425. https://doi.org/10.1016/j.molonc.2011.07.005.

[9] Murakami M, Izumi H, Kurita T, et al. UBE2L6 is involved in cisplatin resistance by regulating the transcription of ABCB6 [J]. Anticancer Agents Med Chem, 2020, 20(12): 1487-1496. https://doi.org/10.2174/1871520620666200424130934.

[10] Zhang J, Zhang X, Li J, et al. Systematic analysis of the ABC transporter family in hepatocellular carcinoma reveals the importance of ABCB6 in regulating ferroptosis[J]. Life Sci, 2020, 257: 118131. https://doi.org/10.1016/j.lfs.2020.118131.

[11] Yin Z, Lv Y, Deng L, et al. Targeting ABCB6 with nitidine chloride inhibits PI3K/AKT signaling pathway to promote ferroptosis in multiple myeloma[J]. Free Radic Biol Med, 2023, 203: 86-101. https://doi.org/10.1016/j.freeradbiomed.2023.04.003.

[12] Dixon SJ, Lemberg KM, Lamprecht MR, et al. Ferroptosis: an iron-dependent form of nonapoptotic cell death[J]. Cell, 2012, 149(5): 1060-1072. https://doi.org/10.1016/j.cell.2012.03.042.

[13] Huang Y, Wang S, Ke A, et al. Ferroptosis and its interaction with tumor immune microenvironment in liver cancer[J]. Biochim Biophys Acta Rev Cancer, 2023, 1878(1): 188848. https://doi.org/10.1016/j.bbcan.2022.188848.

[14] 陶芃作, 蒋玉娥, 王海, 等. CYP2J2介导生成的EETs通过PPARγ促进胰腺导管腺癌铁死亡抵抗[J]. 中南大学学报(医学版), 2021, 46(9): 932-941. https://doi.org/10.11817/j.issn.1672-7347.2021.210413.
TAO Pengzuo, JIANG Yu'e, WANG Hai, et al. CYP2J2-produced epoxyeicosatrienoic acids contribute to the ferroptosis resistance of pancreatic ductal adenocarcinoma in a PPARγ -dependent manner[J]. Journal of Central South University. Medical Science, 2021, 46(9): 932-941. https://doi.org/10.11817/j.issn.1672-7347.2021.210413.

[15] Peng B, Ling X, Huang T, et al. HSP70 via HIF-1α SUMOylation inhibits ferroptosis inducing lung cancer recurrence after insufficient radiofrequency ablation[J/OL]. PLoS One, 2023, 18(11): e0294263[2025-02-14]. https://doi.org/10.1371/journal.pone.0294263.

[16] Zhu Y, Yang L, Yu Y, et al. Hydroxysafflor yellow A induced ferroptosis of Osteosarcoma cancer cells by HIF-1α/HK2 and SLC7A11 pathway[J]. Oncol Res, 2024, 32(5): 899-910. https://doi.org/10.32604/or.2023.042604.

[17] Semenza GL. Targeting HIF-1 for cancer therapy[J]. Nat Rev Cancer, 2003, 3(10): 721-732. https://doi.org/10.1038/nrc1187.

[18] Semenza GL. HIF-1 and mechanisms of hypoxia sensing[J]. Curr Opin Cell Biol, 2001, 13(2): 167-171. https://doi.org/10.1016/s0955-0674(00)00194-0.

[19] 彭再梅, 山长婷, 王惠芳. 肺癌组织中VHL和HIF-1α表达及其临床意义[J]. 中南大学学报(医学版), 2009, 34(4): 331-334. https://doi.org/10.3321/j.issn: 1672-7347.2009.04.011.
PENG Zaimei, SHAN Changting, WANG Huifang. Expression of VHL and HIF-1α and its clinical significance in the lung cancer tissue[J]. Journal of Central South University. Medical Sciences, 2009, 34(4): 331-334. https://doi.org/10.3321/j.issn: 1672-7347.2009.04.011.

[20] Mitsuhashi N, Miki T, Senbongi H, et al. MTABC3, a novel mitochondrial ATP-binding cassette protein involved in iron homeostasis* 210[J]. J Biol Chem, 2000, 275(23): 17536-17540. https://doi.org/10.1074/jbc.275.23.17536.

[21] Chavan H, Khan MM, Tegos G, et al. Efficient purification and reconstitution of ATP binding cassette transporter B6 (ABCB6) for functional and structural studies[J]. J Biol Chem, 2013, 288 (31): 22658-22669. https://doi.org/10.1074/jbc.M113.485284.

[22] Wang C, Cao C, Wang N, et al. Cryo-electron microscopy structure of human ABCB6 transporter[J]. Protein Sci, 2020, 29 (12): 2363-2374. https://doi.org/10.1002/pro.3960.

[23] Lin Z, Wu Z, He Y, et al. CYFIP1 coordinate with RNMT to

©Journal of Central South University (Medical Science). All rights reserved.

induce osteosarcoma cuproptosis via AURKAIP1 M7G modification[J]. Mol Med, 2025, 31(1): 74. https://doi.org/10.1186/s10020-025-01127-3.

[24] 徐雅瑄, 赵欣雨, 高雨雨, 等. 谷氨酰胺代谢重编程调控骨肉瘤发生和发展[J]. 中南大学学报(医学版), 2025, 50(12): 2425-2437. https://doi.org/10.11817/j.issn.1672-7347.2025.250321.
XU Yaxuan, ZHAO Xinyu, GAO Yuyu, et al. Glutamine metabolic reprogramming in regulating the occurrence and development of osteosarcoma[J]. Journal of Central South University. Medical Science, 2025, 50(12): 2425-2437. https://doi.org/10.11817/j.issn.1672-7347.2025.250321.

[25] Zhao L, Zhou X, Xie F, et al. Ferroptosis in cancer and cancer immunotherapy[J]. Cancer Commun, 2022, 42(2): 88-116. https://doi.org/10.1002/cac2.12250.

[26] Mou Y, Wang J, Wu J, et al. Ferroptosis, a new form of cell death: opportunities and challenges in cancer[J]. J Hematol Oncol, 2019, 12(1): 34. https://doi.org/10.1186/s13045-019-0720-y.

[27] Jiang X, Stockwell BR, Conrad M. Ferroptosis: mechanisms, biology and role in disease[J]. Nat Rev Mol Cell Biol, 2021, 22(4): 266-282. https://doi.org/10.1038/s41580-020-00324-8.

[28] Chen X, Kang R, Kroemer G, et al. Broadening horizons: the role of ferroptosis in cancer[J]. Nat Rev Clin Oncol, 2021, 18(5): 280-296. https://doi.org/10.1038/s41571-020-00462-0.

[29] Jiang M, Jike Y, Liu K, et al. Exosome-mediated miR-144-3p promotes ferroptosis to inhibit osteosarcoma proliferation, migration, and invasion through regulating ZEB1[J]. Mol Cancer, 2023, 22(1): 113. https://doi.org/10.1186/s12943-023-01804-z.

[30] Sattiraju A, Kang S, Giotti B, et al. Hypoxic niches attract and sequester tumor-associated macrophages and cytotoxic T cells and reprogram them for immunosuppression[J]. Immunity, 2023, 56(8): 1825-1843. https://doi.org/10.1016/j.immuni.2023.06.017.

[31] He M, Wang Y, Xie J, et al. M7G modification of FTH1 and pri-miR-26a regulates ferroptosis and chemotherapy resistance in osteosarcoma[J]. Oncogene, 2024, 43(5): 341-353. https://doi.org/10.1038/s41388-023-02882-5.

[32] Kelter G, Steinbach D, Konkimalla VB, et al. Role of transferrin receptor and the ABC transporters ABCB6 and ABCB7 for resistance and differentiation of tumor cells towards artesunate[J/OL]. PLoS One, 2007, 2(8): e798[2025-02-14]. https://doi.org/10.1371/journal.pone.0000798.

[33] Yang Z, Su W, Wei X, et al. HIF-1α drives resistance to ferroptosis in solid tumors by promoting lactate production and activating SLC1A1[J]. Cell Rep, 2023, 42(8): 112945. https://doi.org/10.1016/j.celrep.2023.112945.

[34] Yuan S, Wei C, Liu G, et al. Sorafenib attenuates liver fibrosis by triggering hepatic stellate cell ferroptosis via HIF-1α/SLC7A11 pathway[J/OL]. Cell Prolif, 2022, 55(1): e13158[2025-02-14]. https://doi.org/10.1111/cpr.13158.

[35] Shi J, Wang QH, Wei X, et al. Histone acetyltransferase P300 deficiency promotes ferroptosis of vascular smooth muscle cells by activating the HIF-1α/HMOX1 axis[J]. Mol Med, 2023, 29(1): 91. https://doi.org/10.1186/s10020-023-00694-7.

[36] Pugh CW, Ratcliffe PJ. The von Hippel-Lindau tumor suppressor, hypoxia-inducible factor-1 (HIF-1) degradation, and cancer pathogenesis[J]. Semin Cancer Biol, 2003, 13(1): 83-89. https://doi.org/10.1016/s1044-579x(02)00103-7.

[37] Krishnamurthy PC, Du G, Fukuda Y, et al. Identification of a mammalian mitochondrial porphyrin transporter[J]. Nature, 2006, 443(7111): 586-589. https://doi.org/10.1038/nature05125.

[38] Li M, Li L, Cheng X, et al. Hypoxia promotes the growth and metastasis of ovarian cancer cells by suppressing ferroptosis via upregulating SLC2A12[J]. Exp Cell Res, 2023, 433(2): 113851. https://doi.org/10.1016/j.yexcr.2023.113851.

(Edited by SONG Liu)

©Journal of Central South University (Medical Science). All rights reserved.